

In₂O₃-CuO NANO-FLAKES PREPARED BY SPRAY PYROLYSIS FOR GAS SENSING APPLICATION

A. A. KHALEFA^a, J. M. MAREF^b, H. A. RADWAN^b, J. M. RZAIJ^{c,*}

^aMinistry of Education, General Directorate of Salah AL-din Educating

^bMinistry of Education, General Directorate of Kirkuk Educating

^cDepartment of Physics, College of Science, University of Anbar, Ramadi, Iraq

Indium oxide: copper oxide nanoflakes deposited by spray pyrolysis using an aqueous solution of chloride powders at 1:1 indium to copper ions ratio. XRD measurement shows polycrystalline structures of mixed In₂O₃ and CuO phases. The crystallinity enhanced with increasing annealing temperature and an additional ternary phase of In₂Cu₂O₅ appeared at 623 K. AFM measurements illustrate an obvious variation in the morphology of the sample surface with the variation of annealing temperature. The SEM image shows Thin walls connected in the irregular direction created by cavities that gave the sample a high surface area. The sensing measurements against NO₂ gas confirmed the best sample was that prepared at 673 K, where the sensitivity increased while the response and recovery times decreased. The optimum sensitivity appeared at 473 K operating temperature is 55%.

(Received October 9, 2020; Accepted February 12, 2021)

Keywords: In₂O₃, Gas sensor, CuO, Spry pyrolysis, Metal oxide

1. Introduction

Detection of metal oxide gas sensors depends on the absorbed oxygen which is converted to ion species by trapping electrons from the surface of the material [1]. The change in the resistance of the sensor usually occurs due to the interaction between the target gas with the adsorbed oxygen species, which causes the resistance to change as a signal due to the return or extracted additional electrons from the semiconductor surface [2].

To obtain a sensor of high sensitivity, one must study the mechanism of the interaction between the gas (within the lowest concentration) and the surface of the material then convert this reaction to the equivalent changes in the electrical resistance of the sensor [3].

The ternary compounds copper-indium- oxide are known to be attractive in many fields such as in transparency electrodes [4], photodetectors [5], liquid crystal displays [6]. The green (Cu₂In₂O₅) and black (CuIn₂O₄) compounds are formed when the CuO interacts with In₂O₃. [7]. One of the interesting ternary phases is the Cu₂In₂O₅ which crystallized in the orthorhombic system, it is an oxygen-rich phase and can easily be prepared by the solid-state synthesis in the air [8].

Cu₂In₂O₅ belongs to the family of Cu₂R₂O₅ (R=rare earth element) that first received considerable attention as the phases related to high T_c superconductors, as well as it has good magnetic properties. In recent years, there are several reports concerned with the synthesis method using a chemical method and reaction mechanisms for prepared the Cu₂In₂O₅ nanoparticles [9]. It is particularly interesting because it can be doped with p and n-type material allowing p-n homojunction to be produced [10]. The compound Cu₂In₂O₅ can be obtained under appropriate conditions by various techniques, from 1:1 ratio of copper to indium ions, precipitation method [8], doctor-blading [11], and sol-gel spin coating technique [9].

The lack of information on the existence of Cu₂In₂O₅ phase in CuO-In₂O₃ system prepared by spray pyrolysis technique has prompted us to study phases in this system and then study the performance of the prepared films against NO₂ as a gas sensor.

*Corresponding author: sc.jam72al@uonanbar.edu.iq

2. Experimental

Indium oxide: copper oxide (In_2O_3 : CuO) thin composite films of 1:1 copper to indium ions ratio were prepared on glass substrates by spray pyrolysis technique using indium (III) chloride (InCl_3) of 99.999% purity and copper (II) chloride (CuCl_2) of 99.995% purity from Sigma-Aldrich Co. The two powders were dissolved in an equal molar ratio to prepare a 0.1 M solution in distilled water using a magnetic stirrer until a clear solution was obtained. Thin films were sprayed at different temperatures (523–673 K at a step of 50 K). The substrates were placed on a controlled temperature hot plate. The atomizer is set at a height of 25 cm. The solution is sprayed intermittently for 5 seconds, open and closed state, using compressed air of 5 bar pressure. The structural and optical properties of the prepared films were studied by x-ray diffraction and UV-visible absorption respectively. Using atomic force microscopy and scanning electron microscopy, the surface characteristics were identified.

Mesh electrodes were deposited on the surface of the samples by print screen silver paste. Gas sensing was examined in a closed chamber on a hot plate heater attached with a thermocouple connected with a thermometer to control its temperature. The gas target and air mixture flow into the chamber by two flow-meter. The resistance of the sample was measured as a function of the time, in case of on and off the gas, using an electronic circuit connected to a computer.

3. Results and discussions

3.1 X-ray diffraction results

X-ray diffraction patterns for In_2O_3 :CuO thin films prepared by spray pyrolysis on corning glass at different substrate temperatures (523, 573, 623, and 673 K) were shown in Fig. 1.

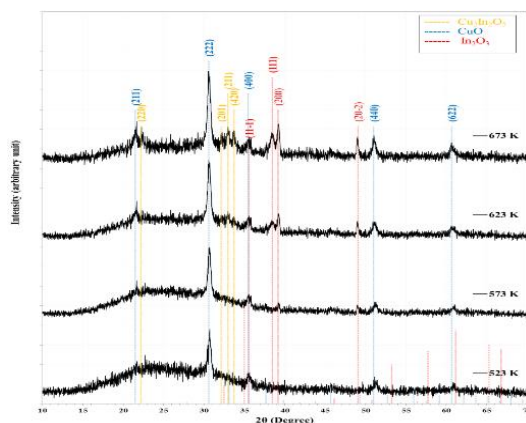


Fig. 1. X-ray diffraction patterns for In_2O_3 :CuO thin films prepared at different substrate temperatures.

The polycrystalline structure appeared with four broad peaks corresponding to the In_2O_3 structure, consistent with card No. 96-101-0589. At 523 K, a low crystallinity was located at diffraction angles $2\theta = 30.70^\circ$, 35.54° , 51.28° , and 60.90° corresponding to (222), (400), (440) and (622) orientation planes respectively. The absence of other phases (CuO and/or $\text{In}_2\text{Cu}_2\text{O}_5$) may be due to the temperature of the substrate was inadequate to crystallize the crystal at this temperature.

Increasing the temperature of the substrate improves the crystalline structure with the appearance of the phase of cupric oxide (CuO) matching the No. 96-410-5683 card. A new phase of $\text{In}_2\text{Cu}_2\text{O}_5$, matched with card No. 96-200-2191, also appeared, and peak intensities were improved.

The appearance of the three phases together without the absence of the CuO phase at this temperature maybe return to that the samples need a higher temperature than used to completely

convert to the ternary compound $\text{In}_2\text{Cu}_2\text{O}_5$, as mentioned by the phase diagram by Bosacka *et al* [7]. The peaks broadening was measured by Lorentzian fitting, as shown in Fig. 2, for the (222) direction of the In_2O_3 structure. The full width at half maximum (FWHM) decreased with increasing the substrate temperature, demonstrating to increase in the crystalline size. Table 1 reveals the diffraction angles (2θ) and the inter-planer distances (d_{hkl} Exp.) which are determined by the Bragg law, while the FWHM and crystalline size (C.S) calculated using Sherrer's formula. It is also showing that the average crystallite size for prepared samples increased as the substrate temperature increased, as shown in Fig. 4.

Table 1. XRD peaks parameters for $\text{In}_2\text{O}_3:\text{CuO}$ thin films prepared at different substrate temperatures.

T_s (K)	2θ (Deg.)	FWHM (Deg.)	d_{hkl} Exp.(Å)	C.S (nm)	Phase	hkl
523	30.70	0.4311	2.9099	19.1	Cubic In_2O_3	(222)
	35.54	0.7838	2.5239	10.6	Cubic In_2O_3	(400)
	51.28	0.6180	1.7802	14.3	Cubic In_2O_3	(440)
	60.90	0.5500	1.5200	16.8	Cubic In_2O_3	(622)
573	30.68	0.4762	2.9118	17.3	Cubic In_2O_3	(222)
	35.54	0.9400	2.5239	8.9	Cubic In_2O_3	(400)
	39.26	0.4236	2.2929	19.9	Monoclinic CuO	(200)
	49.02	0.4110	1.8568	21.2	Monoclinic CuO	(20-2)
	51.24	0.6853	1.7815	12.9	Cubic In_2O_3	(440)
	61.00	0.7110	1.5177	13.0	Cubic In_2O_3	(622)
623	21.66	0.5244	4.0996	15.4	Cubic In_2O_3	(211)
	30.60	0.5370	2.9192	15.3	Cubic In_2O_3	(222)
	35.56	0.6400	2.5226	13.0	Cubic In_2O_3	(400)
	38.36	1.4700	2.3446	5.7	Monoclinic CuO	(111)
	39.22	0.3729	2.2952	22.6	Monoclinic CuO	(200)
	49.00	0.2950	1.8575	29.6	Monoclinic CuO	(20-2)
	51.04	0.5020	1.7880	17.5	Cubic In_2O_3	(440)
	60.60	0.8475	1.5268	10.9	Cubic In_2O_3	(622)
673	21.66	0.4917	4.0996	16.4	Cubic In_2O_3	(211)
	22.20	0.3870	4.0011	20.9	Tet. $\text{Cu}_2\text{In}_2\text{O}_5$	(220)
	30.60	0.4974	2.9192	16.6	Cubic In_2O_3	(222)
	32.15	0.4230	2.7819	19.5	Tet. $\text{Cu}_2\text{In}_2\text{O}_5$	(201)
	32.98	0.4350	2.7138	19.0	Tet. $\text{Cu}_2\text{In}_2\text{O}_5$	(211)
	33.70	0.4120	2.6574	20.1	Tet. $\text{Cu}_2\text{In}_2\text{O}_5$	(420)
	35.56	0.5489	2.5226	15.2	Cubic In_2O_3	(400)
	38.40	0.8582	2.3423	9.8	Monoclinic CuO	(111)
	39.22	0.4922	2.2952	17.1	Monoclinic CuO	(200)
	48.98	0.3062	1.8582	28.5	Monoclinic CuO	(20-2)
	51.04	0.4986	1.7880	17.7	Cubic In_2O_3	(440)
	60.62	0.8236	1.5263	11.2	Cubic In_2O_3	(622)

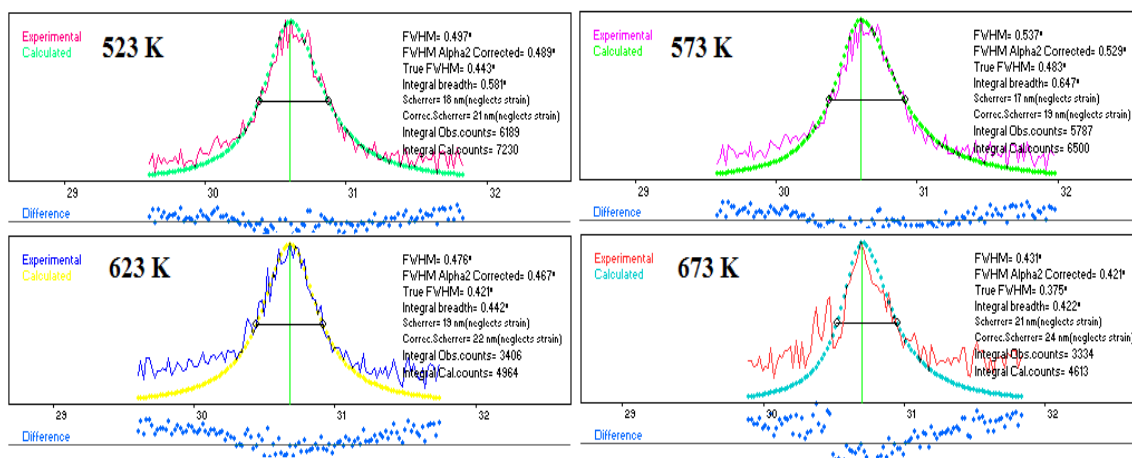


Fig. 2. Lorentzian fitting (using X-powder software) for the preferred direction peak along (222) in the XRD for $\text{In}_2\text{O}_3:\text{CuO}$ thin films prepared at different substrate temperatures.

Two-dimensional x-ray analysis done by X Powder software, revealed in Fig. 3, illustrates that the $\text{Cu}_2\text{In}_2\text{O}_5$ phase maybe appears at temperatures less than 625 K for (211) direction.

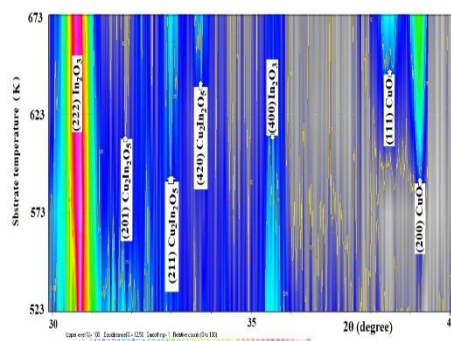


Fig. 3. Two dimensional XRD analysis for $\text{In}_2\text{O}_3:\text{CuO}$ phase variation with substrate temperatures.

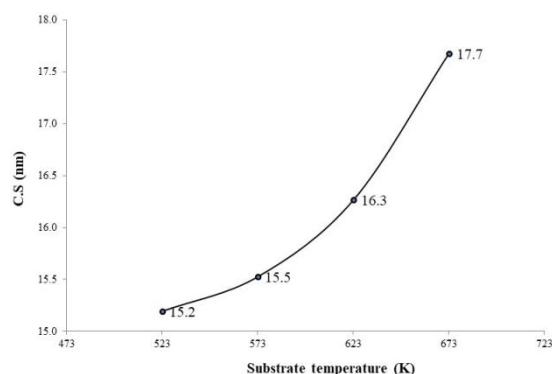


Fig. 4. Variation of average crystalline size with the substrate temperature.

3.2. Atomic force microscopy results

Fig. 5 displays images of the three-dimensional atomic force microscopy and the atom distribution histogram. The particle diameter was calculated using the software Image-J. The particle size started at 523 K uniformly distributed at a wide range of an average value of 106.09

nm and increased with increasing the substrate temperature due to the increase in crystalline growth and the merging of adjacent particles by removing the grain boundaries between them [12]. Fig.5 shows that the particles prepared at a substrate temperature of 673 K are irregularly distributed and have cavities. The average particle diameter was found to increase with an increase in deposition temperature [13], as shown in Table 2, in which the minimum, maximum and average diameter for $\text{In}_2\text{O}_3:\text{CuO}$ particles are tabulated.

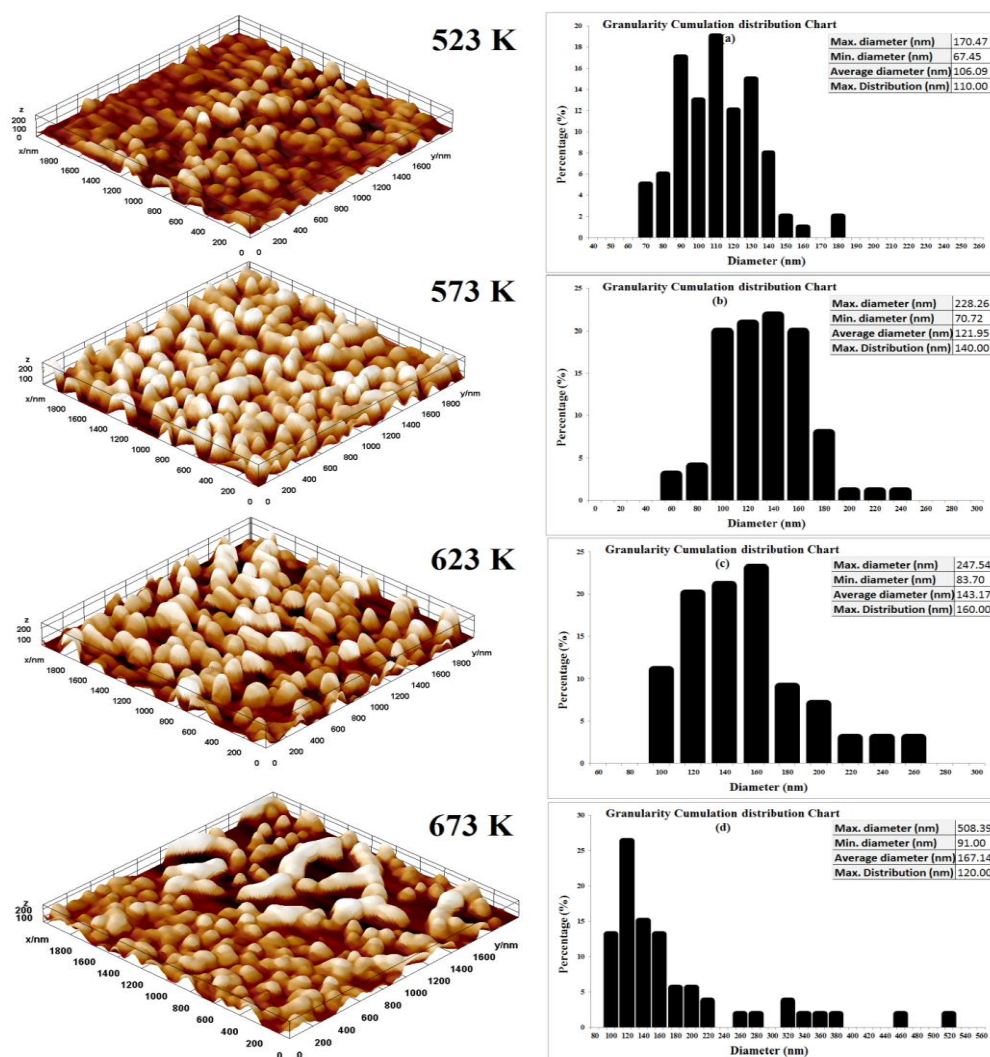


Fig. 5. The 3-D AFM images and particle size distribution for $\text{In}_2\text{O}_3:\text{CuO}$ thin films prepared at different substrate temperatures.

Table 2. Minimum, maximum, and average diameter for $\text{In}_2\text{O}_3:\text{CuO}$ thin films prepared at different substrate temperatures.

Substrate temperature (K)	Minimum diameter (nm)	Maximum diameter (nm)	Average Diameter (nm)
523	67.45	170.47	106.09
573	70.72	228.26	121.95
623	83.70	247.54	143.17
673	91.00	508.39	167.14

3.3 Scanning electron microscopy results

Fig. 6 shows the scanning electron microscope image of the $\text{In}_2\text{O}_3:\text{CuO}$ thin film sample at 673 K substrate temperature. As can be seen, the prepared film surface has a structure ordered of connected thin walls or nano-flakes of irregular directions, creating cavities with different diameters that vary from 230 to 438 nm range. This structure increases the surface area of this sample. In structure, the gas sensing properties always strongly relied on their surface properties and nanostructure shapes, where the sample met the requirement of a great surface to volume ratios [14].

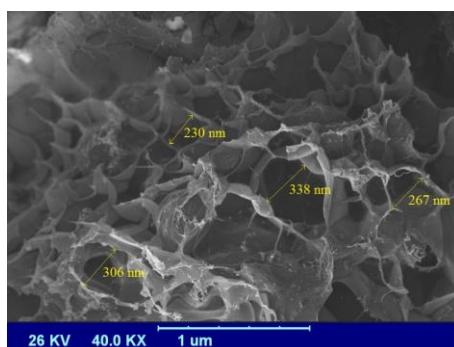


Fig. 6. SEM for $\text{In}_2\text{O}_3:\text{CuO}$ nanoflakes thin film prepared at 673 K substrate temperature.

3.4. Gas sensor analysis

Fig. 7 shows the variation sensor response ($R_{\text{gas}}/R_{\text{air}}$) [15] with time, for gas-on and off, for the $\text{In}_2\text{O}_3:\text{CuO}$ composite samples deposited at different substrate temperatures, when exposed to 10 ppm NO_2 in the air at 473 K operating temperature. The resistance increased when the sample was exposed to the gas, i.e the sample behaves as an n-type to oxidized gas. Fig. 8-a shows that the gas sensitivity, which calculated from $S = (R_{\text{gas}} - R_{\text{air}})/R_{\text{air}} \times 100\%$, was increased with increasing substrate temperature due to the variation of surface morphology, especially at 673 K temperature as shown in AFM and SEM measurements.

The response and recovery time, which also are important parameters for a gas sensor, are defined as the times to reach 90% variation in resistance upon exposure to the gas and air, respectively. The response time of $\text{In}_2\text{O}_3:\text{CuO}$ sensor deposited at 673 K substrate temperature exhibited a shorter response and recovery times for all samples, about 27 and 35 seconds, respectively. The recovery time was slower, possibly due to slow surface reactions, including absorption, dissociation, and ionization of oxygen molecules, compared to the rapid diffusion of the examined gas[16].

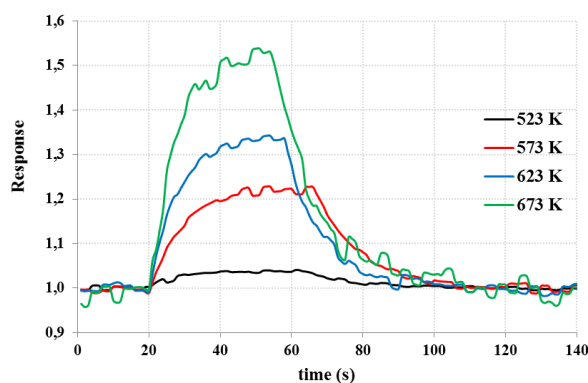


Fig. 7. Variation of sensor response with time for $\text{In}_2\text{O}_3:\text{CuO}$ composite prepared at different substrate temperatures against 10 ppm NO_2 gas.

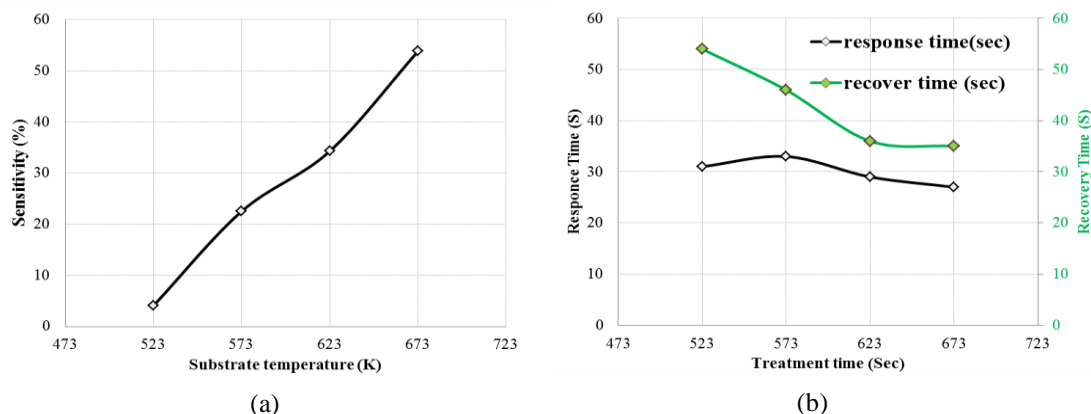


Fig. 8. Variation of (a) NO_2 gas sensitivity (b) response and recovery times, with substrate temperature for $\text{In}_2\text{O}_3:\text{CuO}$ composite thin against 10 ppm NO_2 gas.

Operating temperature is an important factor in gas sensors. Fig. 9 shows the response variation for the $\text{In}_2\text{O}_3:\text{CuO}$ nanoflakes thin film deposited at 673 K substrate temperature when the sample exposed to a 10 ppm NO_2 in the air at different operating temperatures (373, 473, and 573 K). The optimum gas sensitivity was found at 473 K as shown in Fig. 10, due to the variety of oxygen ion species adsorbed on the sample surface that contribute to gas sensitivity processes. At low temperatures, $\text{O}_2^-_{\text{ads}}$ forms on the surface from ambient oxygen attract electrons from the sample. increasing temperature make that dominant reaction is $\text{O}_2^-_{\text{ads}} + e^- = 2\text{O}^-_{\text{ads}}$ [17] which attracts more electrons from the sample, while the higher temperature cause to reduce the adsorbed gases on the sample surface which effect on sample response [18].

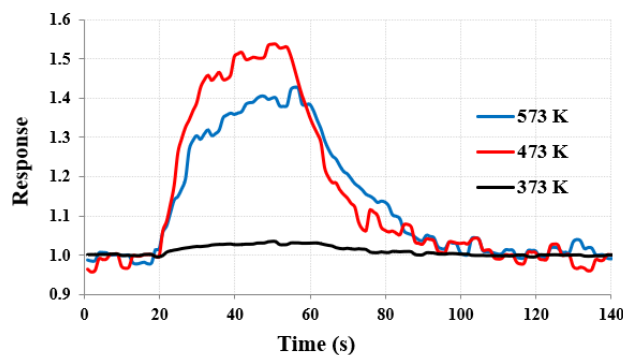


Fig. 9. Variation of sensor response with time for $\text{In}_2\text{O}_3:\text{CuO}$ composite thin films at different operating temperatures against 10 ppm NO_2 gas.

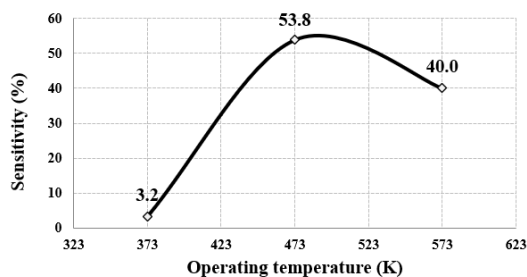


Fig. 10. Variation of NO_2 gas sensitivity against operating temperature for $\text{In}_2\text{O}_3:\text{CuO}$ composite thin against 10 ppm NO_2 gas.

4. Conclusions

NO₂ gas sensor was simply fabricated based on In₂O₃:CuO nanoflakes deposited by spray pyrolysis technique using indium(III) and chloride and copper(II) chloride aqueous solution at a ratio of 1:1. Structural examination shows polycrystalline structures of the two phases In₂O₃ and CuO. The crystallinity increased with increasing annealing temperature and an additional phase of In₂Cu₂O₅ appeared at 623 K substrate temperature. AFM measurements show a variation in surface morphology behavior with increasing annealing temperature, especially at 673 K. SEM image shows structure ordered of connected thin walls creating cavities of high surface area which is a great influence the gas sensitivity. The associated measurements confirmed this behavior, as the sensitivity increased and the response and recovery times decreased when the deposition substrate temperature increased to 623 K. The optimum sensitivity appeared at an operating temperature of 473 K.

References

- [1] R. Sakthivel, P. M. Shameer, *Int. J. Sci. Res.* **183–189**, 4 (2015).
- [2] J. M. Rzaij, A. M. Abass, *J. Chem. Rev.* **114–121**, 2 (2020).
- [3] R. Kumar, G. Kumar, A. Umar, *Nano-Micro Lett.* **97–120**, 7 (2015).
- [4] M. Singh, V. N. Singh, B. R. Mehta, *J. Nanosci. Nanotechnol.* 3889–3894, 8 (2008).
- [5] N. M. Khusayfan, A. A. Al-ghamdi, F. Yakuphanoglu, *J. Alloys Compd.* **796–807**, 663 (2016).
- [6] G. S. Okram, V. Ganesan, R. R. Philip, *J. Alloys Compd.* **435–444**, 746 (2018).
- [7] M. Bosacka, E. Filipek, A. Paczesna, *J. Therm. Anal. Calorim.* **605–610**, 109 (2012).
- [8] C. Su, C. Chiu, C. Chang, J. Ting, *Thin Solid Films* **42–48**, 531 (2013).
- [9] J. Xu, Y. Wan, Y. Huang, Y. Wang, L. Qin, H. Jin, *Appl. Surf. Sci.* **639–644**, 389 (2016).
- [10] C. W. Teplin, T. Kaydanova, D. L. Young, J. D. Perkins, D. S. Ginley, A. Ode, D. W. Readey, C. W. Teplin, T. Kaydanova, D. L. Young, J. D. Perkins, D. S. Ginley, *Appl. Phys. Lett.* **3789**, 85 (2004).
- [11] C. Su, D. K. Mishra, C. Chiu, J. Ting, *Surf. Coat. Technol.* **517–520**, 231 (2013).
- [12] J. M. Rzaij, N. F. Habubi, *Appl. Phys. A* **1–10**, 126 (2020).
- [13] J. C. Hsieh, C. J. Liu, Y. H. Ju, *Thin Solid Films* **98–103**, 322 (1998).
- [14] P. H. Suman, A. A. Felix, H. L. Tuller, J. A. Varela, M. O. Orlandi, *Sensors Actuators B Chem.* **122–127**, 208 (2015).
- [15] K. Schneider, W. Maziarz, *Proceedings* **1–5**, 2 (2018).
- [16] H. Xuemei, S. Yukun, B. Bo, *J. Nanomater.* **1–9**, 2016 (2016).
- [17] L. Francioso, A. Forleo, S. Capone, M. Epifani, A. M. Taurino, P. Siciliano, *Sensors Actuators B* **646–655**, 114 (2006).
- [18] Y. F. Sun, S. B. Liu, F. L. Meng, J. Y. Liu, Z. Jin, L. T. Kong, J. H. Liu, *Sensors* **2610–2631**, 12 (2012).